THE JOURNAL OF BIOLOGICAL CHEMISTRY Vol. 276, No. 40, Issue of October 5, pp. 37630–37639, 2001
Printed in U.S.A.

Investigation of the Catalytic Site within the ATP-Grasp Domain of *Clostridium symbiosum* Pyruvate Phosphate Dikinase*

Received for publication, June 18, 2001
Published, JBC Papers in Press, July 23, 2001, DOI 10.1074/jbc.M105631200

Dongmei Ye‡, Min Wei‡, Marielena McGuire§, Kui Huang¶, Geeta Kapadia¶, Osnat Herzberg¶‖, Brian M. Martin, and Debra Dunaway-Mariano‡‖**

*From the ‡Department of Chemistry, University of New Mexico, Albuquerque, New Mexico 87131, the §Department of Chemistry and Biochemistry, University of Maryland, College Park, Maryland 27042, the ¶Center for Advanced Research in Biotechnology, University of Maryland Biotechnology Institute, Rockville, Maryland 20850, and **Clinical Neuroscience, National Institutes of Health, Bethesda, Maryland 20892*

Pyruvate phosphate dikinase (PPDK) catalyzes the interconversion of ATP, P_i, and pyruvate with AMP, PP_i, and phosphoenolpyruvate (PEP) in three partial reactions as follows: 1) *E*-His + ATP → *E*-His-PP·AMP; 2) *E*-His-PP·AMP + P_i → *E*-His-P·AMP·PP_i; and 3) *E*-His-P + pyruvate → *E*·PEP using His-455 as the carrier of the transferred phosphoryl groups. The crystal structure of the *Clostridium symbiosum* PPDK (in the unbound state) reveals a three-domain structure consisting of consecutive N-terminal, central His-455, and C-terminal domains. The N-terminal and central His-455 domains catalyze partial reactions 1 and 2, whereas the C-terminal and central His-455 domains catalyze partial reaction 3. Attempts to obtain a crystal structure of the enzyme with substrate ligands bound at the nucleotide binding domain have been unsuccessful. The object of the present study is to demonstrate Mg(II) activation of catalysis at the ATP/P_i active site, to identify the residues at the ATP/P_i active site that contribute to catalysis, and to identify roles for these residues based on their positions within the active site scaffold. First, Mg(II) activation studies of catalysis of *E* + ATP + P_i → *E*-P + AMP + PP_i partial reaction were carried out using a truncation mutant (Tem533) in which the C-terminal domain is absent. The kinetics show that a minimum of 2 Mg(II) per active site is required for the reaction. The active site residues used for substrate/cofactor binding/activation were identified by site-directed mutagenesis. Lys-22, Arg-92, Asp-321, Glu-323, and Gln-335 mutants were found to be inactive; Arg-337, Glu-279, Asp-280, and Arg-135 mutants were partially active; and Thr-253 and Gln-240 mutants were almost fully active. The participation of the nucleotide ribose 2′-OH and α-P in enzyme binding is indicated by the loss of productive binding seen with substrate analogs modified at these positions. The ATP, P_i, and Mg(II) ions were docked into the PPDK N-terminal domain crevice, in an orientation consistent with substrate/cofactor binding modes observed for other members of the ATP-Grasp fold enzyme superfamily and consistent with the structure-function data. On the basis of this docking model, the ATP polyphosphate moiety is oriented/activated for pyrophosphoryl transfer through interaction with Lys-22 (γ-P), Arg-92 (α-P), and the Gly-101 to Met-103 loop (γ-P) as well as with the Mg(II) cofactors. The P_i is oriented/activated for partial reaction 2 through interaction with Arg-337 and a Mg(II) cofactor. The Mg(II) ions are bound through interaction with Asp-321, Glu-323, and Gln-335 and substrate. Residues Glu-279, Asp-280, and Arg-135 are suggested to function in the closure of an active site loop, over the nucleotide ribose-binding site.

Pyruvate phosphate dikinase (PPDK)[1] catalyzes the interconversion of ATP, P_i, and pyruvate with AMP, PP_i, and PEP in the presence of Mg^{2+} and NH_4^+ ion activators (1). The reaction takes place in three steps, each of which requires the participation of His-455. As shown in Scheme 1, His-455 abstracts the γ,β-PP-unit from ATP and then, in the two subsequent steps, delivers a phosphoryl group to P_i and then to pyruvate. Kinetic studies have indicated that catalysis of the first two steps (*E*·ATP·P_i → *E*-PP·AMP·P_i → *E*-P·AMP·PP_i) and catalysis of the third step (*E*-P·pyruvate → *E*·PEP) occurs at separate active sites (2, 3). The x-ray crystal structure of the *Clostridium symbiosum* apoPPDK (4) revealed that the 96-kDa enzyme is organized into three consecutive domains that are connected by two flexible linkers (Fig. 1*A*). Affinity labeling and mutagenesis studies have shown that the N-terminal domain binds ATP (5, 26) and P_i (6) and that the C-terminal domain binds pyruvate (7, 27). The catalytic His-455, on the other hand, is located on the surface of the central domain. During the catalytic turnover, His-455 must move from the active site located at the N-terminal domain to the active site located at the C-terminal domain. This movement can be modeled by rotating the two solvated interdomain linkers, which allows the central domain to swivel from the concave surface of the N-terminal domain to that of the C-terminal domain (see modeled structure shown in Fig. 1*B*) (4).

An extensive search for conditions that facilitate the co-crystallization of PPDK, nucleotide, P_i, and Mg(II) has been made but so far without success. Thus, whereas the x-ray structure of apoPPDK has been known for some time (4), the locations of substrate and cofactor-binding sites within the N-terminal domain active site crevice have not been determined. The object of the present study is to measure Mg(II)

* This work was supported by National Institutes of Health Grant GM 36260 (to D. D.-M.) and National Science Foundation Grant MCB9813271 (to O. H.). The costs of publication of this article were defrayed in part by the payment of page charges. This article must therefore be hereby marked "*advertisement*" in accordance with 18 U.S.C. Section 1734 solely to indicate this fact.

The atomic coordinates and structure factors (code 1JDE) have been deposited in the Protein Data Bank, Research Collaboratory for Structural Bioinformatics, Rutgers University, New Brunswick, NJ (http://www.rcsb.org/).

‖ To whom correspondence should be addressed. Tel.: 505-277-3776; Fax: 505-277-2609; E-mail: dmye@unm.edu.

[1] The abbreviations used are: PPDK, pyruvate phosphate dikinase; AMPPNP, 5′-adenylimidodiphosphate; PEP, phosphoenolpyruvate; HPLC, high performance liquid chromatography.

activation of catalysis at the ATP/P_i active site, to identify the residues that contribute to catalysis at this site, and to derive probable functional roles for these residues based on their positions within the active site scaffold.

EXPERIMENTAL PROCEDURES

Site-directed Mutants—Mutant genes were prepared from the plasmid pACYC184-D12 (9) using a polymerase chain reaction-based procedure analogous to that described previously (6). Mutagenic primers, 18–22 base pairs in length, were synthesized by Life Technologies, Inc. *Bgl*II and *Bst*XI restriction sites were employed in the construction of the T253A, E279A, D280A, Q240A, R135A, R92A, R92K, K22A, and K22R PPDK mutants, whereas *Bst*XI and *Kpn*I restriction sites were used in the construction of the E323D, E323L, D321N, and Q335A mutants. The sequence analyses of the mutant genes were carried out by the Center for Agricultural Biotechnology at the University of Maryland. Wild-type and mutant PPDK genes were expressed in *Escherichia coli* JM101 cells, and the protein products were purified to homogeneity (as judged by SDS-polyacrylamide gel electrophoresis analysis) as described previously (6) in yields of 8–25 mg/g cell. Each mutant is stable to chromatography and storage. The only exception is the D321N mutant, which is susceptible to hydrolytic cleavage. After 3 weeks of storage in 50 mM K^+Hepes buffer (pH 7.0) at 4 °C, 60% of the D321N mutant had undergone the fragmentation process described previously (7, 27).

N-terminal Domain-Central Domain PPDK Mutant Protein (Tem533)—The mutant gene, encoding residues 1–533 in PPDK, was prepared and expressed as described above. The protein was purified in a yield of 4 mg/g cell. Its N-terminal sequence, determined by automated protein sequencing, is identical to that of the wild-type PPDK. The molecular mass of Tem533 was determined by matrix-assisted laser desorption ionization-mass spectrometry at the University of Michigan Protein and Carbohydrate Structure Facility to be 58.6 ± 0.2 kDa. This value compares well with the theoretical molecular mass of 58,654 Da. The molecular mass of the native protein was determined by gel column chromatography to be ~51 kDa. Thus, the mutant protein is monomeric.

Spectrophotometric Assay—Initial velocities were measured as a function of the concentration of the varied substrate (in a range of 0.5–10-fold K_m) at fixed, saturating concentrations of cosubstrates (0.5 mM AMP, 0.5 mM PEP, 1 mM PP_i) and metal ion cofactors (5 mM $MgCl_2$ and 40 mM NH_4Cl) in 20 mM imidazole (pH 6.8, 25 °C). The initial velocity data were analyzed using Equation 1 and the computer programs of Cleland (10). The k_{cat} value was calculated from $V_{max}/[E]$.

$$V_o = V_{max}[S]/(K_m + [S]) \quad \text{(Eq. 1)}$$

where V_o is the initial velocity; [*E*] is the enzyme concentration; [S] is the substrate concentration; V_{max} is the maximum velocity, and K_m is the Michaelis constant.

The K_i values for the competitive inhibitor AMPPNP were determined from initial velocity data obtained at varying AMP concentrations and fixed, saturating concentrations of cosubstrates and cofactors. The initial velocity data were analyzed using Equation 2 where K_i is the inhibition constant and [I] is the inhibitor concentration.

$$V_o = V_{max}[S]/[K_m(1 + [I]/K_i) + [S]] \quad \text{(Eq. 2)}$$

Radioisotopic Assay—Reaction solutions (100 μl) initially containing 30 μM enzyme, 1 mM [^{14}C]AMP, 1 mM PP_i, 1 mM PEP, 5 mM $MgCl_2$, 40 mM NH_4Cl, 0.2 mM NADH, 20 units/ml lactate dehydrogenase in 50 mM K^+Hepes (pH 7.0, 25 °C) were quenched at specific times with 300 μl of 0.6 M HCl. The protein was removed by centrifugal filtration (500 μl Microsep filter; 10-kDa cut off). The [^{14}C]ATP and [^{14}C]AMP were separated from the supernatant by HPLC using a 4.6-mm × 25-cm Beckman ultrasphere C18 reversed-phase analytical column and 25 mM KH_2PO_4, 2.5% triethylamine, and 5% methanol as eluant (1 ml/min flow rate). Peak fractions were quantitated by scintillation counting.

ATP + P_i + Pyruvate → AMP + PP_i + PEP Reaction—Reaction solutions (100 μl) initially containing 0.1–20 μM enzyme, 5 mM pyruvate, 5 mM P_i, 5 mM $MgCl_2$, 40 mM NH_4Cl, and 20 units/ml of inorganic pyrophosphatase (to drive the reaction to completion by catalyzing PP_i hydrolysis) in 50 mM K^+Hepes (pH 7.0, 25 °C) were quenched at specified times with 300 μl of 0.6 M HCl. The resulting solutions were filtered and analyzed by HPLC as described above.

Mg(II) Activation of Tem533—The time courses ([^{14}C]AMP concentration *versus* reaction time) for wild-type and Tem533 PPDK-catalyzed single turnover reactions of *E* +[^{14}C]ATP → *E*-PP·AMP and *E* + [^{14}C]ATP + P_i → *E*-P + [^{14}C]AMP + PP_i were carried out as described previously (6). The time courses ([^{14}C]AMP concentration *versus* reaction time) used for the determination of the k_{obs} *versus* [Mg(II)] plot were measured with 60-μl reaction solutions initially containing 40 μM [^{14}C]ATP, 40 μM Tem533 PPDK, and variable $MgCl_2$ concentration (10–5000 μM) in 40 mM NH_4Cl and 50 mM K^+Hepes (pH 7.0, 25 °C). The reactions were terminated and analyzed for [^{14}C]AMP and [^{14}C]ATP as described previously (6). The k_{obs} was calculated from the time course data using Equation 3, where P_t is the concentration of [^{14}C]AMP at time *t,* and P*eq* is the concentration of [^{14}C]AMP at equilibrium.

$$\log P_t/P_{eq} = k_{obs}(t) \quad \text{(Eq. 3)}$$

X-ray Crystallographic Analysis of K22A PPDK—The crystallization conditions used for the *C. symbiosum* K22A PPDK mutant were the same as those used for the wild-type enzyme (4). Single crystals were obtained at 30 °C by vapor diffusion in hanging drops. Protein drops

E + ATP → E•ATP → E-PP•AMP *Partial Reaction 1*

E-PP•AMP + P_i → E-PP•AMP•P_i → E-P•AMP•PP_i *Partial Reaction 2*

E-P + pyruvate → E-P•pyruvate → E-P•PEP *Partial Reaction 3*

SCHEME 1. **The partial reactions catalyzed by PPDK (8).**

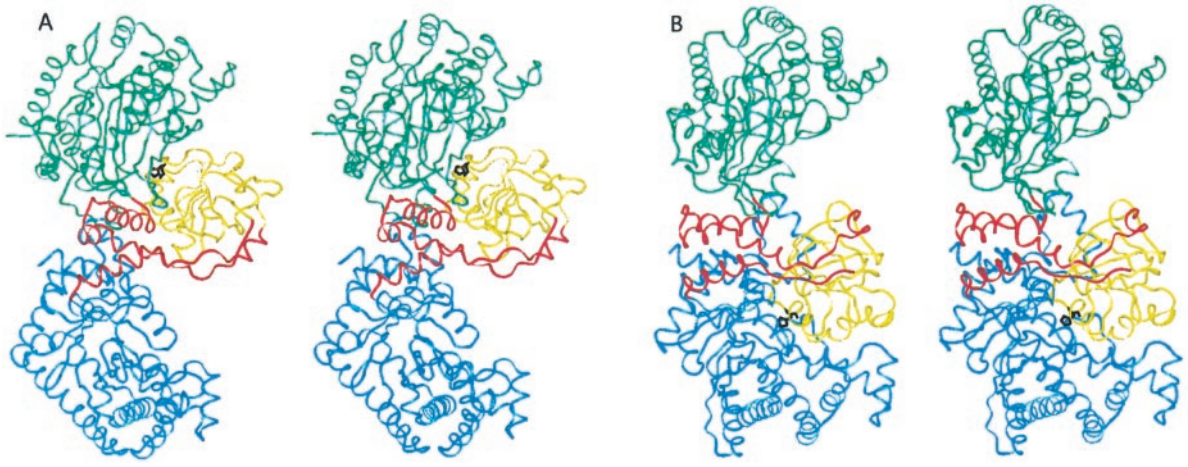

FIG. 1. *A,* conformer 1, ribbon stereodiagram of the *C. symbiosum* PPDK monomer generated from the x-ray coordinates of the apoPPDK structure reported previously (4) using INSIGHTII. Catalysis of the *E* + ATP + P_i → *E*-P + AMP + PP_i partial reactions takes place at the N-terminal domain (*green*) active site in conformer 1. *B,* conformer 2, ribbon stereodiagram of the *C. symbiosum* PPDK monomer modeled from the structure shown in *A.* Catalysis of the *E*-P + pyruvate → *E* + PEP partial reaction takes place at the C-terminal domain (*blue*) active site in the modeled conformer 2. Movement of the catalytic His-455 residue (*black*) between the two active sites is perceived to occur through the interconversion of conformers 1 and 2 via the swivel of the central domain (*yellow*) about its helical linkers (*red*) (4).

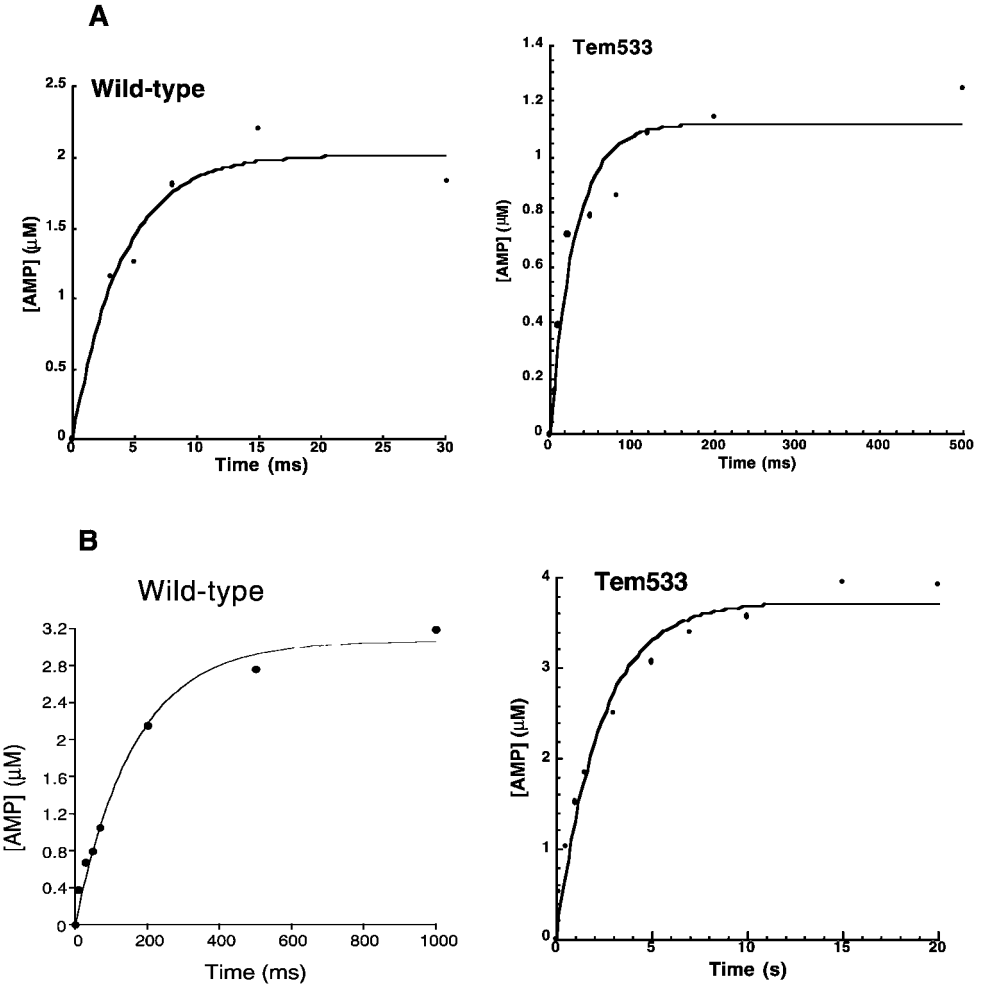

FIG. 2. *A,* the time course for E + [^{14}C]ATP → E-PP·[^{14}C]AMP single turnover reaction catalyzed by wild-type (*left*) and Tem533 (*right*) PPDK. Initial reaction solutions contained 40 μM enzyme, 10 μM [^{14}C]ATP, 2.5 mM $CoCl_2$, 40 mM NH_4Cl, and 50 mM K^+Hepes (pH 7.0, 25 °C). *B,* the time course for E + [^{14}C]ATP + P_i → E-P·[^{14}C]AMP·PP_i single turnover reaction catalyzed by wild-type (*left*) and Tem533 (*right*) PPDK. Initial reaction solutions contained 20 μM enzyme, 5 μM [^{14}C]ATP, 11 mM P_i, 5 mM $MgCl_2$, 40 mM NH_4Cl, and 50 mM K^+Hepes (pH 7.0, 25 °C).

were equilibrated against reservoir solutions containing 50–55% saturated ammonium sulfate and 100 mM Hepes buffer, pH 7.0. The drops consisted of protein at ~10 mg/ml, 20 mM imidazole buffer, pH 6.5, 100 mM KCl, 0.1 mM EDTA, and 1 mM mercaptoethanol diluted by an equal volume of reservoir solution. The crystals belong to the space group P_2, and within the accuracy of the data the unit cell dimensions are the same as those of the wild-type protein crystals (Table IV). X-ray diffraction data were collected on a Siemens area detector mounted on a 3-circle goniostat, with monochromated CuK_α x-ray supplied by a Rigaku Rotaflex RU200BH rotating anode generator. Data were processed with the XENGEN package (11). Data collection statistics are provided in Table IV. Initial structure refinement was performed with the program X-PLOR (12). The simulated annealing slow-cooling protocol at 3000 K was followed by positional refinement cycles. Data between 8.0 and 2.8 Å for which $F \geq 3\sigma(F)$ were included. Adjustments to the model were made on a Silicon Graphics INDIGO II computer graphics work station using the program TURBO-FRODO (13). The later stages of refinement were performed with the program TNT (14) including data between 10 and 2.8 Å for which $F \geq 2\sigma(F)$. The refinement results are summarized in Table IV.

RESULTS

Mg(II) Activation—The N-terminal domain of PPDK has a fold similar to the folds of the ATP binding domains of the ATP-Grasp enzyme superfamily. The members of this superfamily bind, and activate, ATP for γ-P phosphoryl transfer to a variety of cosubstrates (15). PPDK, which catalyzes pyrophosphoryl transfer by displacement at the ATP β-P, represents a point of chemical divergence within the family. Aside from PPDK, each member of the ATP-Grasp family is known to bind one or more divalent metal ions at the catalytic site, and all but synapsin (which binds a single Ca(II) ion) utilizes Mg(II) as the physiological cofactor. PPDK requires Mg(II) for catalysis (1). Based on previous studies of the Mg(II) dependence of PPDK catalyzed isotope exchange, there is evidence that suggests that Mg(II) is a required cofactor at both active sites (16, 17).

The object of this study was to measure Mg(II) activation at the N-terminal domain active site. For this purpose, the truncation mutant Tem533 (PPDK residues 1–533), in which the C-terminal domain has been deleted, was used in place of native PPDK. Since the Tem533 does not contain the PEP/pyruvate active site, Mg(II) binding at the ATP/P_i site of Tem533 may be studied without the interference from Mg(II) binding at the PEP/pyruvate site.

The Tem533 PPDK mutant gene was constructed by site-directed mutagenesis and expressed in *E. coli* cells to provide 4 mg of purified protein/g of cells. The efficiency of catalysis of the E + ATP → E-PP·AMP and E + ATP + P_i → E-P + AMP + PP_i partial reactions was measured in the presence of saturating Mg(II) (5 mM). The rate data are plotted in Fig. 2. The k_{obs} values, determined by fitting the time course data to a single exponential equation (Equation 3) (Table I), indicate that Tem533 PPDK has retained 10% of the activity of the native enzyme. At the present, the reason behind the 10-fold reduction in catalytic efficiency is not known. We suspect, however, that substrate binding and product release from the

TABLE I
The observed rate constants (k_{obs}) derived from single turnover reactions catalyzed by wild-type (WT) and Tem533 PPDK

Reaction	$^{WT}k_{obs}$	$^{Tem533}k_{obs}$
	s^{-1}	
E + [^{14}C]ATP[a]	300	25
E + [^{14}C]ATP + P_i[b]	6.5	0.4

[a] The initial reaction mixture contained 40 μM enzyme, 10 μM [^{14}C]ATP, 2.5 mM $CoCl_2$, 40 mM NH_4Cl, and 50 mM K^+Hepes (pH 7.0, 25 °C). The k_{obs} values were obtained from fitting the rate data of Fig. 2*A* to Equation 3. The k_{obs} = 300 s^{-1} listed for wild-type PPDK is only an estimate since the data points defining the initial portion of the time course curve are lost within the mixing time of the rapid quench instrument.

[b] The initial reaction mixture contained 20 μM enzyme, 5 μM [^{14}C]ATP, 11 mM P_i, 5 mM $MgCl_2$, 40 mM NH_4Cl, and 50 mM K^+Hepes (pH 7.0, 25 °C). The k_{obs} values were obtained from fitting the rate data of Fig. 2*B* to Equation 3.

N-terminal domain active site require that the central domain is docked at the C-terminal domain. Nonetheless, the Tem533 mutant was sufficiently active to carry out the Mg(II) activation studies as planned.

The E + ATP + $P_i \rightarrow E$-P + AMP + PP_i partial reaction, and not the E + ATP $\rightarrow E$-PP·AMP partial reaction, was chosen to measure Mg(II) activation. This is because the level of product formation in the E + ATP $\rightarrow E$-PP·AMP partial reaction is small (5% (17)) when Mg(II) is used as cofactor (note that the Co(II) used in the reaction reported in Fig. 2*A* serves to increase product formation to 25% owing to tighter ATP binding and greater E-PP·AMP stability (17)). The E + ATP + $P_i \rightarrow E$-P + AMP + PP_i partial reaction, on the other hand, is driven to 65% completion (Fig. 2*B*) by P_i, independent of the cofactor used. The higher the level of the product formation, the more accurate is the product determination. The rate (k_{obs}) of the E + ATP + $P_i \rightarrow E$-P + AMP + PP_i partial reaction was measured using 40 μM enzyme to react with 40 μM [^{14}C]ATP in the presence of 11 mM P_i. A similar data set was obtained using 1 mM P_i. The Mg(II) concentrations used in the reaction ranged from 0 to 5 mM. The plot of k_{obs} *versus* [Mg(II)], shown in Fig. 3*A*, deviates from the hyperbolic curve predicted for single site Mg(II) binding. Several determinations of k_{obs} were carried out for reactions containing between 0 and 100 μM [Mg(II)] in order to define an apparent "lag" in enzyme activation observed at the low concentration range (Fig. 3*B*).

The presence of a lag in the k_{obs} *versus* [Mg(II)] of plot (Fig. 3) may be explained by a two-site Mg(II) binding model. Specifically, one site on the enzyme binds Mg(II) with high affinity, whereas the second site binds Mg(II) with significantly lower affinity.[2] The absence of product formation at Mg(II) concentrations below ~80 μM, followed by a "hyperbolic" response between the rate of product formation and the Mg(II) concentration in the 100–5000 μM range, suggests that a high affinity site is being titrated at low Mg(II) concentration (*i.e.* on the order of the enzyme concentration = 40 μM), and once this first site is filled Mg(II) is available to bind to the second site. Only when both sites are occupied is the enzyme competent to catalyze the reaction.

[2] A model in which ATP binds one Mg(II) and the Mg(ATP), in turn, binds to the enzyme is also consistent with these data. The second Mg(II) binds then to the apoenzyme and/or to the enzyme-Mg(ATP) complex. In addition, since the "break in the lag" occurs at a Mg(II) concentration of 80 μM and the enzyme is present at a concentration of 40 μM, it is possible that two high affinity sites and one low affinity site exist on the enzyme. The present data are, however, not sufficient to make a distinction between one and two high affinity sites. Future studies, focused on metal activation of PPDK, will examine cofactor stoichiometry more thoroughly than can be done in this work.

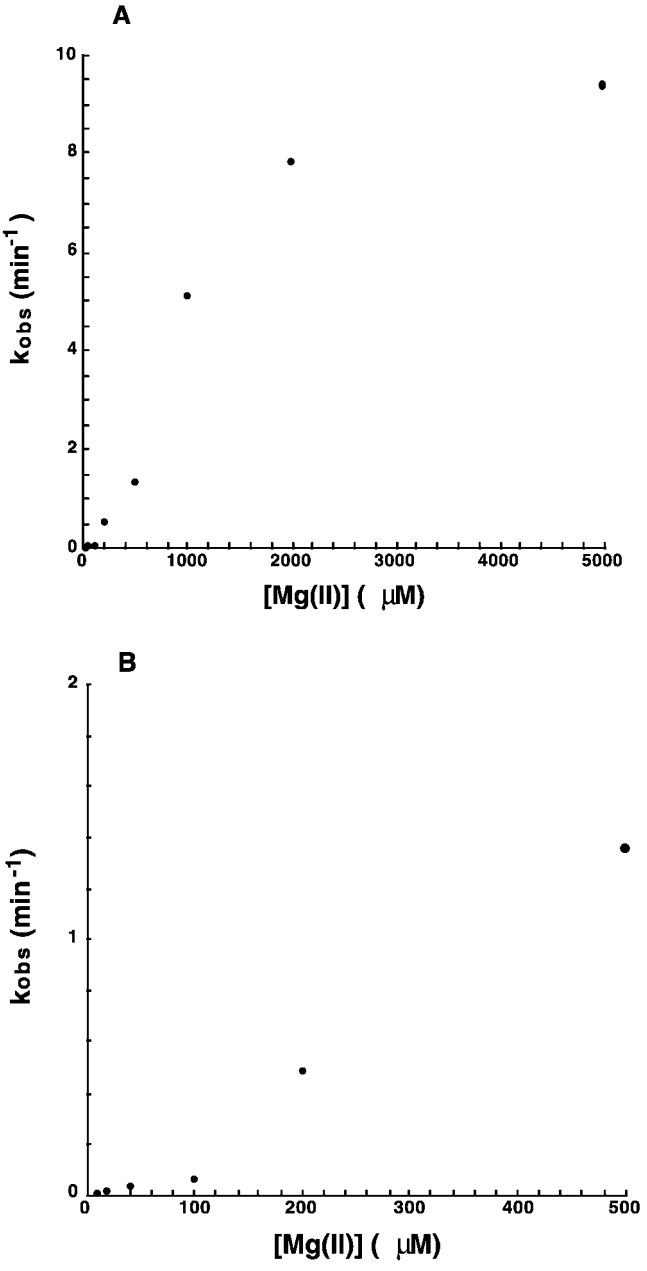

FIG. 3. *A,* plot of k_{obs} *versus* [Mg(II)]. Reaction solutions used to measure k_{obs} initially contained 40 μM Tem533, 40 μM [^{14}C]ATP, 11 mM P_i, 40 mM NH_4Cl, 50 mM K^+Hepes (pH 7.0; 25 °C) and $MgCl_2$ 0–5 mM. *B,* expanded region of the plot k_{obs} *versus* [Mg(II)] shown in *A*.

Kinetic Properties of Active Site Mutants—The amino acid residues whose polar side chains project into the ATP/P_i active site crevice include Gln-240, Arg-92, Lys-22, Thr-253, Asp-321, Glu-323, Gln-335, and Arg-337 (Fig. 4). There are also two loops (the 101–103 loop and the 278–281 loop) that contribute to the active site. The 101–103 loop (Gly-101 to Met-102 to Met-103), which is reminiscent of the classical phosphate binding loop observed in other nucleotide-dependent enzymes, is located to one side of the crevice entrance. The 278–281 loop (containing residues Glu-279 and Asp-280 whose side chains project into the active site) will be referred to as the "ω-loop." This loop forms the roof of the active site crevice, but in the apoPPDK crystal structure the ω-loop is seen to protrude into the active site, where Glu-279 forms an ion pair with active site residue Arg-92. Substrate binding must displace the loop, thus allowing Glu-279 or Asp-280 to favorably interact with Arg-135 (which may function to hold the loop over the active site)

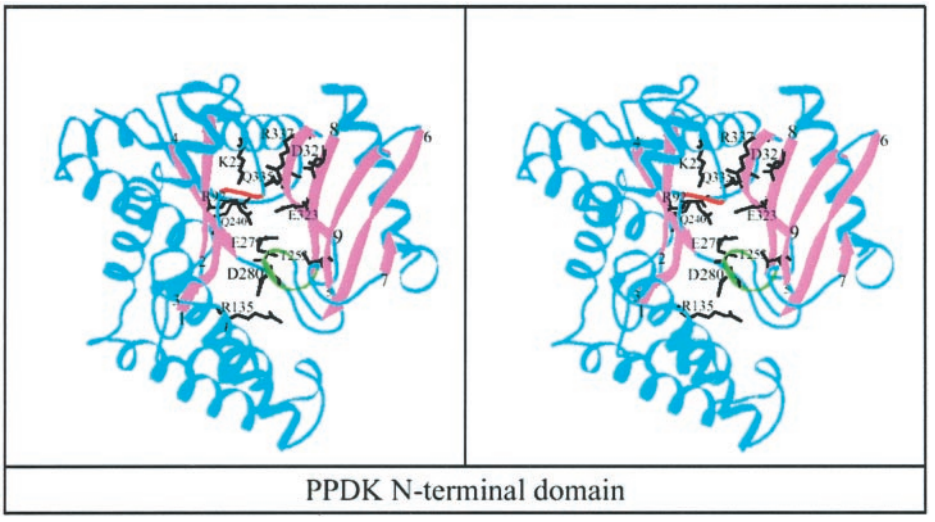

FIG. 4. **Stereodiagram of the N-terminal domain (residues 2–340) observed in the x-ray structure of apoPPDK (4) generated by using the program Molscript.** The *pink* β-strands forming the ATP-Grasp motif are numbered 1–9 (as they are referred to in the text), and the connecting loops which contribute to the active site are shown in *cyan*. Two special loops, the ω-loop (residues 278–281 *colored green*) and the 101–103 loop (*colored red*) are also shown. The side chains of polar residues that contribute to the active site are shown in *black* and are numbered according to their position in the amino acid sequence. These residues are Lys-22, Arg-92, Gln-240, Thr-253, Glu-279, Asp-280, Asp-321, Glu-323, Gln-335, and Arg-337. Arg-135, a potential docking site for the ω-loop, is also shown.

instead of with Arg-92 (which appears to draw the loop into the active site).

Amino acid replacements[3] were made at Gln-240, Arg-92, Lys-22, Thr-253, Asp-321, Glu-323, Gln-335, Arg-337, Glu-279, and Asp-280 in order to determine if these residues contribute to catalysis at the ATP/P_i active site. The mutant enzymes were purified to homogeneity and then evaluated for catalytic activity by measuring their k_{cat} and K_m values using steady-state kinetic techniques. Although the k_{cat} value is determined by the rate at which catalysis occurs at the C-terminal domain active site (Scheme 1, *partial reaction 3*) as well as by the rate at which catalysis occurs at the N-terminal domain active site (*partial reactions 1* and *2*), previous studies (17) have shown that these two rates are comparable in magnitude. Thus, a mutation that significantly slows down catalysis at the N-terminal domain active site will result in a significant reduction in the k_{cat} value measured for the complete reaction.

The mutants were first tested for catalysis of AMP + PP_i + PEP → ATP + P_i + pyruvate reaction using a continuous spectrophotometric assay. Although applicable only to mutants having >0.1% of the wild-type activity, the assay allows easy determination of substrate k_{cat} and K_m values as well as the K_i values of the inert ATP analog AMPPNP (Table II). Less active mutants (R92A, R92K, K22A, D321N, E323D, Q335A, and E279A/D280A) were analyzed using a fixed time, radioisotopic assay. Here, the k_{cat} was determined from the initial velocity measured at fixed substrate concentrations, which for the wild-type enzyme are saturating (Table II). Since amino acid replacement may significantly alter the substrate binding affinity, the assumption that the fixed substrates saturate the mutant enzymes may not hold. Thus, it is possible that the k_{cat} values measured for some of these mutants under-estimate the true k_{cat} values.

Catalysis was also measured in the ATP + P_i + pyruvate → AMP + PP_i + PEP reaction direction using a fixed time, radioisotopic assay (Table III). Only the more active mutants (R135A, D280A, and E279A) were subjected to an initial velocity study to evaluate k_{cat} and $^{ATP}K_m$.

Based on the kinetic values shown in Tables II and III, it can be seen that amino acid replacement at Lys-22, Arg-92, Asp-321, Glu-323, and Gln-335 severely inhibits catalytic turnover. The activities of these mutants are too low for the measurement of K_m or K_i values. Thus, all that can be said about these mutants is that they are inactive.

Mutation at Arg-337 inhibits but does not preclude catalysis (6). The R337A mutant is 18-fold less active in the ATP-forming direction and 520-fold less active in the AMP-forming direction[4] (Tables II and III). The 13-fold increase observed in the $^{PPi}K_m$ value suggests that PP_i and P_i binding may be seriously impaired. Consistent with this deduction is the observation, from transient kinetic studies, that the rate of the E + ATP → E-PP·AMP step is reduced only 5-fold in the R337A mutant, whereas the rate of the E-PP·AMP + P_i → E-P + AMP + PP_i step is reduced 140-fold (6).

The Q240A and T253A mutants have k_{cat} values that are 80 and 50% that of the wild-type enzyme. This suggests that these two residues do not play significant roles in substrate activation. On the other hand, in both cases, the Ala substitution does have some inhibitory effect, as indicated by the 2–10-fold increase seen for $^{AMP}K_m$, $^{PPi}K_m$, and $^{AMPPNP}K_i$ values.

Substitution of the ω-loop residues Glu-279 and Asp-280 and, the putative loop docking site residue, Arg-135 resulted in significant but not severe reductions in catalytic efficiency. The double-loop mutant E279A/D280A, however, is devoid of activity. Measured in the AMP-forming direction, the R135A and E280A mutants showed an 8- and 5-fold reduction in k_{cat}, whereas the E279A mutant showed a 55-fold reduction (Table III). In the ATP-forming direction, k_{cat} is 4-fold smaller in the R135A and E280A mutants and 10-fold smaller in the E279A mutant (Table II). Interestingly, the $^{AMP}K_m$ and $^{AMPPNP}K_i$ values increased 10-fold in the R135A mutant and 2-fold in the D280A mutant. Perhaps these three residues affect catalysis and substrate binding by modulating loop closure and, hence, active site desolvation.

Electronic and Structural Changes in the Active Site Mutants—The replacement of a charged active site amino acid residue with an uncharged one will necessarily perturb the local electrostatic environment, in addition to removing the potential for favorable ligand interaction (*viz.* hydrogen bond formation with substrate or coordination bond formation with Mg(II)). Given that bonding is sensitive to orientation effects, it is sometimes possible to distinguish the role of a charged residue in bonding from that of maintaining an electrochemical

[3] Ala substitution did not affect enzyme solubility. The E323L mutant had been prepared previously in the laboratory and was used here in place of the E323A mutant. The D321N and E323D mutants were used to examine the effects of a comparatively subtle change in side chain structure. For all but one of the positively charged amino acids (*viz.* Arg-135), substitutions with conserved charge were also made.

[4] In the AMP-forming direction, P_i binding will become the limiting factor as the $^{Pi}K_m$ value for the Arg-337 mutant (for wild-type PPDK the $^{Pi}K_m$ = 0.3 mM (2)) will exceed the 5 mM concentration of P_i used in the reaction.

TABLE II
Steady-state kinetic constants measured for wild-type and mutant PPDK catalysis of the AMP + PP_i + PEP → ATP + P_i + pyruvate reaction

The kinetic values are defined within 10% error.

PPDK	k_{cat}	$^{AMP}K_m$	$^{PP}{}_iK_m$	$^{PEP}K_m$	$^{AMPPNP}K_i$
	s^{-1}			μM	
Wild type[a]	25	9.0	89	27	70
Q240A[a]	21	45	370	ND	400
T253A[a]	9.4	85	230	33	140
R135A[a]	6.4	80	156	21	800
E279A[a]	2.0	3.0	40	7.8	110
D280A[a]	6.7	19	87	19	290
R337A[a,b]	1.4	6.0	1140	27	ND
R337K[a,b]	10	6.0	470	21	ND
E279A/D280A[a]		No detectable activity			
R92A[c]	1.3×10^{-4}				
R92K[c]	3.7×10^{-5}				
Q335A[c]	8.6×10^{-5}				
K22A[c]	3.2×10^{-4}				
D321N[c]	1.4×10^{-4}				
E323D[c]	8.3×10^{-4}				
E323L[a]		No detectable activity			

[a] The spectrophotometric assay was used. All reaction solutions contained 5 mM $MgCl_2$ and 40 mM NH_4Cl in 20 mM imidazole HCl (pH 6.8, 25 °C) and were monitored for pyruvate formation using the spectrophotometric coupled assay Ref. 9. For $^{PEP}K_m$ determination, reaction solutions contained varying PEP concentrations at 1.0 mM PP_i and 0.5 mM AMP. For $^{AMP}K_m$ and $^{AMPPNP}K_i$ determinations, reaction solutions contained varying AMP and AMPPNP concentrations at 1.0 mM PP_i and 0.5 mM PEP. For $^{PP}{}_iK_m$ determinations, reaction solutions contained varying PP_i concentrations at 0.5 mM AMP and 0.5 mM PEP.

[b] Kinetic data are from Ref. 6.

[c] Reaction solutions initially containing 1 mM [^{14}C]AMP, 1 mM PP_i, 1 mM PEP, 5 mM $MgCl_2$, and 40 mM NH_4Cl in 20 mM imidazole HCl (pH 6.8, 25 °C) were assayed using the HPLC-based assay for [^{14}C]ATP and [^{14}C]AMP.

TABLE III
Steady-state kinetic constants measured for wild-type and mutant PPDK catalysis of the ATP + P_i + pyruvate → AMP + PP_i + PEP reaction

The kinetic values listed are defined within 10% error.

	k_{cat}	$^{ATP}K_m$
	s^{-1}	μM
Wild type[a]	8.3	190
R135A[a]	1.0	410
D280A[a]	1.6	190
E279A[a]	1.5×10^{-1}	81
E323D[b]	2.1×10^{-3}	
D321N[b]	2.7×10^{-3}	
Q335A[b]	6.5×10^{-5}	
R92A[b]	1.7×10^{-4}	
R92K[b]	No detectable activity	
K22A[b]	2.2×10^{-3}	
K22R[b]	6.4×10^{-3}	
R337A[b,c]	1.6×10^{-2}	
R337K[b,c]	1.7×10^{-1}	

[a] Reaction solutions initially containing varying amounts of ATP, 5 mM pyruvate, 5 mM P_i, 20 units/ml inorganic pyrophosphatase, 5 mM $MgCl_2$, 40 mM NH_4Cl in 50 mM K^+Hepes (pH 7.0, 25 °C) were monitored using the HPLC-based assay for ATP and AMP.

[b] Reaction solutions initially containing 2 mM [^{14}C]ATP, 5 mM pyruvate, 5 mM P_i, 20 units/ml inorganic pyrophosphatase, 5 mM $MgCl_2$, 40 mM NH_4Cl in 50 mM K^+Hepes (pH 7.0, 25 °C) were monitored using the HPLC-based assay for [^{14}C]ATP and [^{14}C]AMP.

[c] Kinetic data are from Ref. 6.

balance, by comparing the kinetic properties of neutral *versus* charged mutants. Here, we examine the three positively charged active site residues Lys-22, Arg-92, and Arg-337.[5] In Tables II and III, the kinetic properties of K22A *versus* K22R PPDK, R92A *versus* R92K PPDK, and R337A *versus* R337K PPDK are compared. In the cases of Lys-22 and Arg-92, the charge-conserving mutants are not significantly more active than are the Ala mutants, thus suggesting that the side chains of the Lys-22 and Arg-92 residues must not only be charged but must also be precisely oriented for substrate activation. Substitution of Arg-337 with Lys results in a 10-fold smaller reduction in catalysis than does substitution with Ala. However, the activity gain with the Lys residue is offset by the loss of chemical specificity. With the R337K mutant, but not the R337A mutant, phosphoryl transfer to water competes with the normal reaction pathway (6). Thus, precise orientation of the charged group at position 337 is also required for efficient catalysis.

The possibility that the replacement of one amino acid with another will trigger a change in active site structure is always a concern. For this reason we attempted to obtain x-ray crystal structures of each of the site-directed mutants. So far the structures of the apoK22A mutant (shown in Fig. 5 and Table IV) and the apoR337A mutant (reported in Ref. 6) have been determined. In both cases, the integrity of the ATP/P_i active site, as it is seen in the original structure of the wild-type apoPPDK (4), is preserved. Thus, at least with these two mutants, we can reasonably attribute the alterations observed in their kinetic properties solely to electronic effects and, more precisely, to the positioning of the charged side chain.

Kinetic Properties of Substrate Analogs—Nucleotide analogs, having modified base, ribose, or phosphate moieties, were tested as substrates and competitive inhibitors. The k_{cat} and K_m, or K_i values obtained from steady-state kinetic measurements are listed in Table V. The AMP analogs, IMP and GMP, are not active substrates nor are they effective inhibitors. Thus, we conclude that PPDK has a strict specificity for the adenine ring. Adenosine 5′-monophosphorothioate and adenosine 5′-monosulfate are also inactive as substrates. The adenosine 5′-monosulfate displays little binding affinity, whereas the adenosine 5′-monophosphorothioate shows a modest degree of binding (K_i = 310 μM *versus* K_d = 50 μM AMP (17)). These findings are suggestive of direct binding interaction between the α-P and the enzyme. The k_{cat} and K_m values of 3′-deoxy-ATP are close to those of ATP, whereas reduced k_{cat} and increased K_m values are observed for 2′-deoxy-ATP, 2′-deoxy-

[5] The same comparison can be made for the Asp-321 and Glu-323 mutants although our kinetic data are not complete. Both E323D and E323L catalytic activities are severely impaired. In the E323D mutant, a carboxyl side chain is present but its "reach" has been reduced. Thus, we conclude that side chain orientation is important at this position.

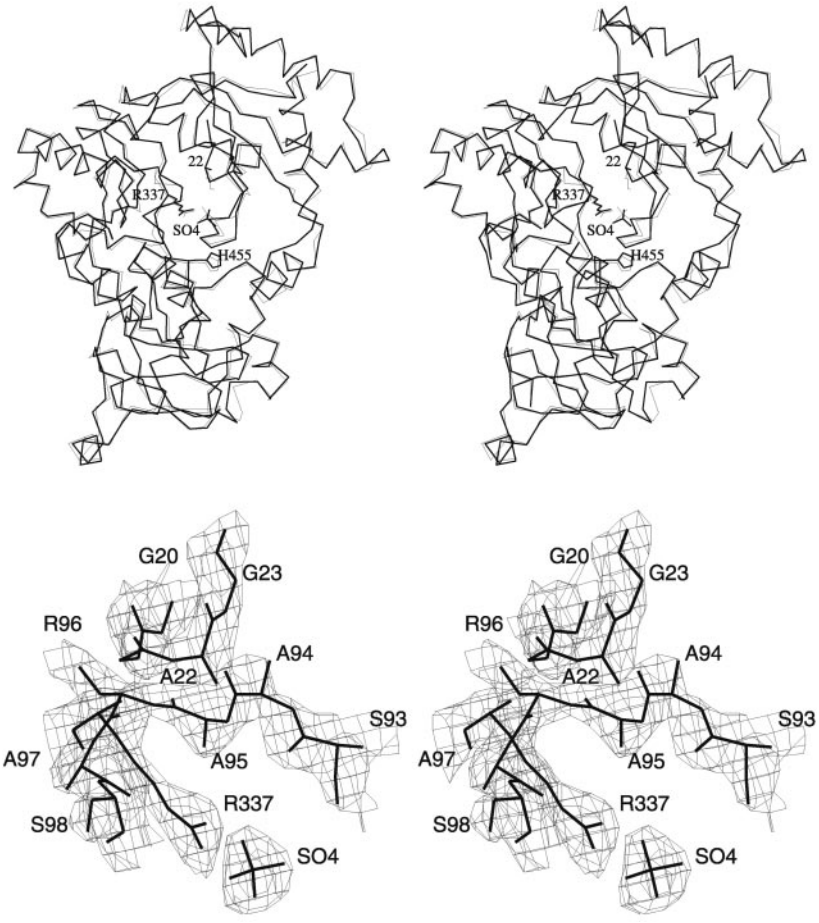

FIG. 5. *Top,* superposition of the K22A PPDK (*thick lines*) and wild-type PPDK (*thin lines*) N-terminal (ATP/P_i binding) and central (catalytic His-455) domains. The residues 534–874 comprising the C-terminal domain as well as residues 109–200 of the N-terminal subdomain 2 (not part of the ATP-Grasp fold) are not included in the structure. *Bottom,* electron density map showing the mutation site of the K22A PPDK mutant. The map is contoured at 1.2-σ level with map coefficients ($2F_o - F_c$) and calculated phases.

TABLE IV
Statistics of x-ray crystallographic data collection for K22A PPDK

Data collection	
Space group	$P2_1$
Cell parameters	a = 89.9 Å; b = 58.6 Å; c = 102.3 Å β = 95.1°
Maximum resolution (Å)	2.8
No. of crystals used	1
No. of observations	58,293
No. of unique reflections	25,068
R_{merge}[a]	0.07
Completeness (%)	98
	53 (2.9–2.8 Å)
Structure refinement	
R-factor[b]	0.193
No. of reflections	20,093 (10–2.8 Å, $F \geq 2\sigma(F)$)
Root mean square deviation from standard stereochemistry	
Bond length (Å)	0.019
Bond angle (°)	2.7
Planary group (Å)	0.019
No. of protein atoms	6719
No. of solvent	43 (2 sulfate ions)
Root mean square deviation from wild-type PPDK (1DIK) on Cα atoms (Å)	
	0.6

[a] $R_{merge} = \Sigma_{hkl}[(\Sigma_i|I_i - \langle I\rangle|)/\Sigma_i I_i]$, for symmetry equivalent reflections.
[b] R-factor = $\Sigma_{hkl}[|F_o| - |F_c|]/\Sigma_{hkl}|F_o|$.

AMP, and 2′,3′-dideoxy-ATP. These results indicate that the ribose 2′-hydroxy group, but not the 3′-hydroxy group, is important for productive binding.

TABLE V
Kinetic constants measured for ATP/AMP analogs as alternate substrates or as competitive inhibitors of PPDK versus AMP

The kinetic values listed are defined within 10% error.

Ligand	k_{cat}	K_m	K_i
	s^{-1}		μM
ATP[a]	8.3	190	
2′-dATP[a]	1.1×10^{-1}	350	
3′-dATP[a]	6.7	250	
2′,3′-didATP[a,b]	4.4×10^{-2}	280	
AMP[c]	25	9	50[d]
2′-dAMP[c]	1.6	100	
AMPPNP[b,e]			70
AMPS[b,e]			310
AdeS[b,e]			$>1 \times 10^4$
Ade[e]			320
GMP[e,f]			8700
IMP[e]			$>1 \times 10^4$

[a] Reactions initially containing varying nucleotide concentration, 5 mM P_i, 5 mM pyruvate, 5 mM $MgCl_2$, and 40 mM NH_4Cl in 50 mM K^+Hepes (pH 7.0, 25 °C) were monitored using the HPLC-based assay for nucleotide substrate and product.
[b] 2′,3′-didATP, 2′,3′-dideoxyadenosine 5′-triphosphate; AMPS, adenosine 5′-mono-*O*-phosphorothioate; AdeS, adenosine 5′-sulfate.
[c] Reactions initially containing varying nucleotide concentration, 1.0 mM PP_i, 0.5 mM PEP, 5 mM $MgCl_2$, and 40 mM NH_4Cl in 20 mM imidazole HCl (pH 6.8, 25 °C) were monitored using the spectrophotometric coupled assay for pyruvate.
[d] K_d values were determined from a Scatchard plot of equilibrium dialysis data (17).
[e] Reactions initially containing 5–50 μM AMP, 1.0 mM PP_i, 0.5 mM PEP, 5.0 mM $MgCl_2$, and 40 mM NH_4Cl in 20 mM imidazole HCl (pH 6.8, 25 °C) at fixed inhibitor concentration were monitored using the spectrophotometric coupled assay for pyruvate.
[f] Noncompetitive inhibition was observed: K_{is} = 8.7 mM and K_{ii} = 25 mM.

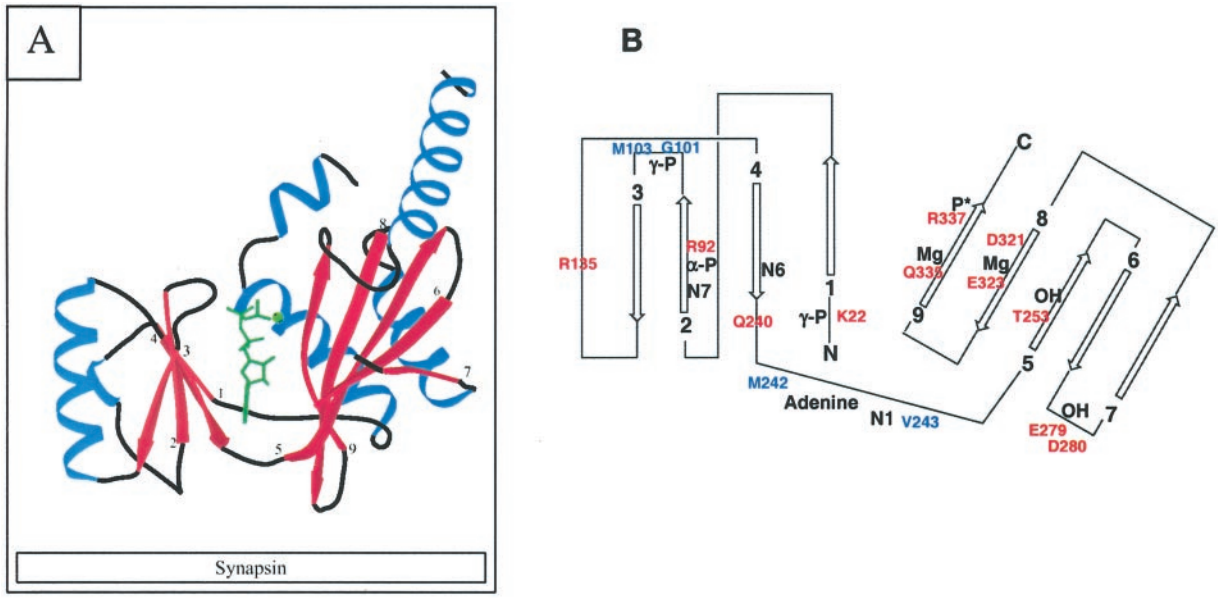

FIG. 6. *A,* ribbon diagram of a ATP-Grasp prototype, synapsin (residues 223–417) in complex with [γ-S]adenosine 5′-triphosphorothioate and Ca(II). The diagram was generated from the coordinates reported previously (22) using Molscript. The nucleotide ligand is shown in *green*, β-strands in *red*, α-helices in *cyan,* and loops in *black.* The individual β-strands comprising the core of the ATP-Grasp motif are labeled *1–9*. Residues 329–343 of the loop connecting β-strands 6 and 7 are disordered in the crystal and, therefore, are not shown. *B,* topological diagram of the ATP-Grasp motif illustrating common functional positions observed among a majority of the members catalyzing γ-phosphoryl transfer. The sites of interaction (*colored black*) are ribose 2′-OH and/or 3′-OH (*OH*), adenine ring (adenine ring, N1, N7, or C(6)NH_2), polyphosphate moiety (α-P, β-P, γ-P; *P** is γ-P in carbamoyl-phosphate synthetase, whereas in PPDK this site is used to bind the cosubstrate P_i), and Mg(II) cofactor (*Mg*). The sites of mutated PPDK residues are colored *red*, whereas those believed contribute to binding (Val-243 backbone C=O) or substrate desolvation (Met-242), but that were not mutated, are colored *blue.*

DISCUSSION

Essential Groups—Based on the substrate analog results (Table V), we propose that the adenine ring, ribose 2′-hydroxy group, and α-phosphate group of ATP participate in productive nucleotide binding. The results from the Mg(II) activation studies (Fig. 3) suggest that a minimum of two Mg(II) cofactors participate in substrate activation. Mutagenesis studies show that the active site residues Gln-240 and Thr-253 play no significant role in catalysis. The ω-loop residues Asp-280 and Glu-279, along with Arg-135 which resides outside of the active site crevice, contribute to catalytic efficiency but are not critical for product formation. Gln-335, Asp-321, Glu-323, Lys-22, and Arg-92 are essential for catalysis and are thus, directly (through ion pair formation; Lys-22 and Arg-92) or indirectly (through Mg(II) coordination, Gln-335, Asp-321, and Glu-323), required for ATP binding/activation. From previous studies (6) it is known that Arg-337 contributes modestly to ATP activation (5-fold rate contribution) and more significantly (140-fold rate contribution) to P_i activation.

Active Site Model—The results summarized above are used, in conjunction with analogies drawn with the ligand binding modes observed for other ATP-Grasp enzymes, to construct a model for ATP, P_i, and Mg(II) binding within the PPDK N-terminal domain active site. The ATP-Grasp family includes PPDK, D-Ala-D-Ala ligase (18, 28), glutathione synthetase (19), carbamoyl-phosphate synthetase (20), succinyl-CoA synthetase (21), synapsin (22), glycinamide ribonucleotide synthetase (23), PurT-encoded glycinamide ribonucleotide transformylase (24), and biotin carboxylase (25, 29). Common to each of these enzymes is the nucleotide binding crevice formed between a 4-stranded antiparallel β-sheet of one subdomain and a 5-stranded antiparallel β-sheet of the other (see the synapsin structure shown in Fig. 6*A* for a clear example of the ATP Grasp-motif). The side chains and backbone amide groups that function in ATP, cosubstrate, and Mg(II) binding are stationed along these 9 β-strands and along the connecting loops. Despite the low degree of sequence homology existing between these enzymes,[6] the conservation of the active site scaffold and the positioning of polar groups for substrate/cofactor binding on this scaffold is remarkably high. This fact has been noted by others (4, 18–25, 28, 29).

In Fig. 6*B*, a generalized topological diagram is provided for the purpose of illustrating the use of common stations for positioning binding/catalytic groups within the ATP-Grasp active sites of the family members. It is based on this common station usage that one can generate an active site model, from the structure of the unbound form of a new family member, with reasonable certainty. However, in drawing an analogy between the ATP-Grasp active sites observed in the family members listed above and that of PPDK, it is necessary to keep in mind the difference in the chemistries involved. Specifically, whereas most members catalyze γ-phosphoryl transfer from ATP to a cosubstrate, PPDK catalyzes two transfers at this active site: first the transfer of the βPγP unit by attack of the carrier His-455 at the β-P of ATP and then the γ-P transfer from the His-455-βPγP to the cosubstrate, P_i. Thus, one might anticipate that some modification of the basic ATP-Grasp active site would be manifested in PPDK. The active site model derived for PPDK is shown in a three-dimensional structural format (derived from the apoPPDK x-ray coordinates (4)) in Fig. 7*A* and in a schematic format in Fig. 7*B*.

Stations for Binding the Adenine Ring—In each ATP-Grasp enzyme, the substrate adenine ring binds (in an anti-conformation) at the apex of the crevice formed between β-sheet 1 (strands 1–4) and β-sheet 2 (strand 5–9) (see synapsin-ATP

[6] The identity is too low, in fact, for useful sequence alignments to be made. Instead, common sites for substrate and cofactor-binding residues have been identified by superpositioning the three-dimensional structures (18–25, 28, 29).

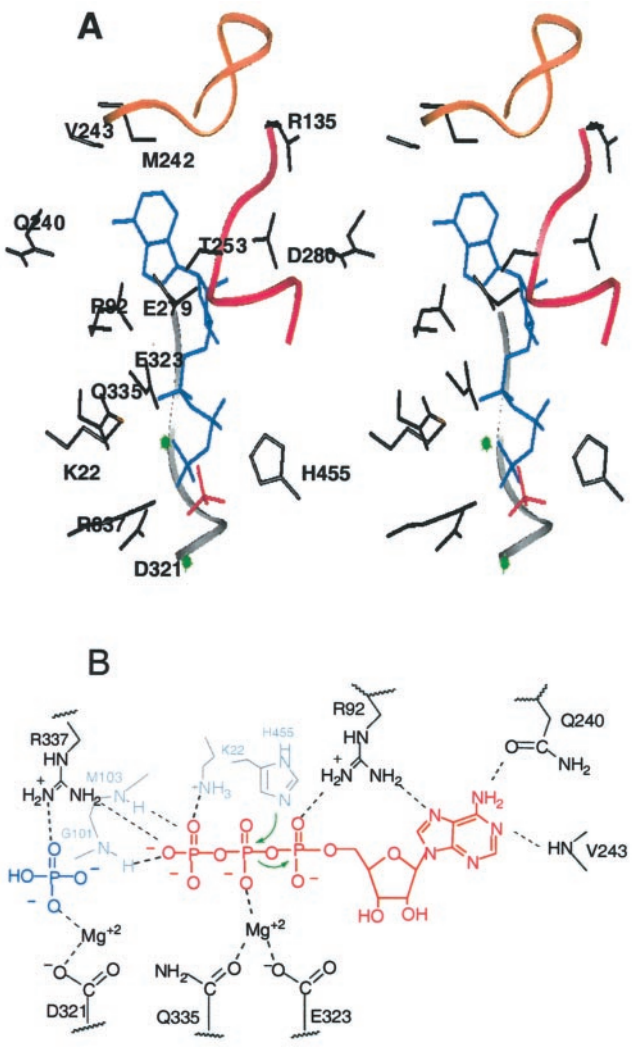

FIG. 7. *A,* stereodiagram of the proposed PPDK N-terminal domain active site model. ATP (*blue*), P_i (*red*), and two Mg(II) ions (*green*) are shown with the side chains (*black*) as well as with the $\beta6$–$\beta7$ ω-loop (*red*; contains Glu-279 and Asp-280), the $\beta2$–$\beta3$ 101–103 loop (*gray;* backbone amide NHs of Gly-101 and Met-103 hydrogen bond with γ-P), and the $\beta4$–$\beta5$ loop (*gold;* backbone amide NH of Val-243 hydrogen bonds with N(1)). *B,* schematic illustration of the interactions between PPDK active site residues, substrates, and Mg(II) ions.

complex shown in Fig. 6*A*). Here, it interacts through N(7) with a Lys or Arg residue stationed on β-stand 2, through C(6)NH_2 with the side chain C=O of an Asp, Glu, or Gln and/or backbone C=O at the C-terminal end of β-strand 4, and through N(1) with main chain amide groups of residues residing on the loop connecting β-strand 4 with β-strand 5 (loop 4–5) (see locations of conserved catalytic stations in Fig. 6*B*). Additionally, the nonpolar side chains of residues located on loop 4–5 pack against the adenine ring, providing hydrophobic interaction and, in some cases, π-π interaction.

By analogy to these structures, the adenine ring of ATP was docked within the PPDK active site crevice in the anti-conformation (see the PPDK active site side chains interacting with modeled ligands in Fig. 7*A*). This orientation allows interaction to occur between the backbone amide NH of Val-243 and the adenine N(1) and between the side chain of Arg-92 and the adenine N(7). The C(6)NH_2 of the adenine ring resides 4.6 Å from the amide group of Gln-240, too distant for hydrogen bond formation. Indeed, replacement of Gln-240 with Ala had no impact on the turnover rate and only a modest effect on substrate binding.

The PPDK Leu-107, Met-242, and Leu-334 side chains surround the adenine ring, thus providing the hydrophobic component of substrate binding observed with the other ATP-Grasp enzyme-nucleotide complexes and suggested by lack of substrate activity and the decreased binding affinity observed for the polar adenine ring analogs GMP and IMP.

Stations for Binding the Ribose Ring—In each ATP-Grasp fold enzyme, the substrate ribose ring is bound in a 2′-endo, 3′-exo conformation (see ribose of ATP ligand bound to synapsin shown in Fig. 6*A*). In some, but not all, ATP-Grasp enzymes, the side chain of an active site Asp or Glu residue, located at the N terminus of β-strand 5, interacts with the 2′-OH and/or 3′-OH (see topological diagram in Fig. 6*B*). In PPDK, this position is occupied by Thr-253. Two family members, D-Ala-D-Ala ligase and glutathione synthetase, also use backbone amide groups of the loop connecting β-strand 6 with β-strand 7 (corresponding to the ω-loop in PPDK) to bind the ribose moiety. The ATP ribose was modeled into the PPDK active site in the 2′-endo, 3′-exo conformation, to obtain a good fit (*i.e.* if one ignores the misplaced ω-loop) (Fig. 7*A*). The ribose 2′-OH resides in the vicinity of Thr-253 of β-strand 5, but it is not optimally positioned to engage in hydrogen bond interaction. Indeed, mutation of Thr-253 to Ala resulted in only a modest reduction in catalytic efficiency. The ribose of the modeled ATP occupies the region that is filled by the β-strand 6-β-strand 7 (ω) loop in the crystal structure of the apoPPDK. We suspect, based on the demonstrated importance of the ribose 2′-OH and of the ω-loop residues Glu-279 or Asp-280, that the loop (through interaction with Arg-135) may function to cap the roof of the active site while possibly binding with the ribose of the nucleotide ligand.

Stations for Binding the Mg(II) Cofactors—Within the active sites of the ATP-Grasp enzymes, the polyphosphate moiety of the bound ATP interacts with one, two, or three divalent metal ion cofactors (18–25, 28, 29). The metal ion-binding residues are, in turn, located on β-strands 8 and 9 (Fig. 6*B*). In PPDK, the three essential residues Glu-323, Asp-321, and Gln-335 are positioned on these strands. These three residues, along with the ATP polyphosphate moiety and P_i, are probable ligands for the Mg(II) cofactors, as we have indicated in the PPDK active site model of Fig. 7*A*. Whereas the Mg(II) sites shown in this model meet spatial restrictions, they are at this stage highly speculative. Moreover, the positions of the Mg(II) ions in partial reaction 1 may change for partial reaction 2. Nevertheless, for catalysis of partial reaction 1, we assume that one Mg(II) is positioned to coordinate with Glu-323 and Gln-335 of the enzyme and with the β-P and γ-P of the ATP ligand. The second Mg(II) is shown to bridge the Asp-321 carboxylate and the P_i ligand.

Stations for Binding the Polyphosphate Chain—Fig. 6*B* shows that the phosphoryl groups of nucleotides bound to ATP-Grasp domains interact with a Lys or Arg located on β-strand 2 (α-P), with the backbone amide NHs of a segment of the loop connecting β-strand 2 with β-strand 3 (β-P) and, in some cases, with the side chain of a Lys or Arg residue located on this same loop. In some of the ATP-Grasp domains, the α-helical segment leading into the N terminus of β-strand 1 is additionally used to position an interacting Lys or Arg side chain. The polyphosphate moiety of the modeled ATP in PPDK interacts with the side chains of Arg-92 (β-strand 2; α-P) and Lys-22 (α-helical segment leading N terminus of β-strand 1; γ-P) and with the backbone amide NHs of Gly-101 and Met-103 (the 101–103 loop connecting β-strand 2 with β-strand 3; γ-P) (Fig. 7*A*). Amino acid replacement at position Lys-22 or Arg-92 precludes reac-

tion with the ATP,[7] suggestive of their important roles in ATP orientation/activation. The Gly-101—Met-102—Met-103 loop (^{98}SMPGMM^{103}) is conserved in all 17 known PPDK sequences, attesting to the importance of this loop in PPDK catalysis. The loop is somewhat more open in the PPDK structure than are the analogous loops observed in the other family members. The alteration in loop conformation seen in PPDK provides for interaction with the γ-P which has been rotated into a unique position. This switch in function, namely using the 101–103 loop in binding the ATP γ-P rather than β-P, is necessary to accommodate the change in location of the transfer reaction from the γ-P to the β-P. The position occupied by the γ-P in the typical ATP-Grasp active site (see for instance, the synapsin structure of Fig. 6*A*) is proposed to be filled by the cosubstrate P_i (Fig. 7) in PPDK. Thus, the use of a station on β-strand 9 (Arg-337), for cosubstrate (P_i) binding, is also unique to PPDK. In carbamoyl-phosphate synthetase for example, this position is filled with an Arg residue that interacts with the ATP γ-P (19).

Conclusions—Presently, our search for conditions that will facilitate the co-crystallization of PPDK with substrate and cofactor ligands for x-ray structure determination continues. We offer the active site model represented in Fig. 7, *A* and *B*, as a reasonable estimate of the mode of substrate and cofactor binding within the ATP/P_i active site. From this model it is evident that PPDK catalysis evolved with minimal alteration of the basic ATP-Grasp active site scaffold.

Acknowledgments—We thank Dr. Fraser and Dr. Wolodoko for early release of the succinyl-CoA synthetase coordinates.

REFERENCES

1. Wood, H. G., O'Brien W, E., and Micheals, G. (1977) *Adv. Enzymol. Relat. Areas Mol. Biol.* **45,** 85–155
2. Wang, H. C., Ciskanik, L., Dunaway-Mariano, D., von der Saal, W., and Villafranca, J. J. (1988) *Biochemistry* **27,** 625–633
3. Thrall, S. H., and Dunaway-Mariano, D. (1994) *Biochemistry* **33,** 1103–1107
4. Herzberg, O., Chen, C. C., Kapadia, G., McGuire, M., Carroll, L. J., Noh, S. J., and Dunaway-Mariano, D. (1996) *Proc. Natl. Acad. Sci. U. S. A.* **93,** 2652–2657
5. Carroll, L. J., Xu, Y., Thrall, S. H., Martin, B. M., and Dunaway-Mariano, D. (1994) *Biochemistry* **33,** 1134–1142
6. McGuire, M., Huang, K., Kapadia, G., Herzberg, O., and Dunaway-Mariano, D. (1998) *Biochemistry* **37,** 13463–13474
7. Xu, Y., Yankie, L., Shen, L., Jung, Y. S., Mariano, P. S., Dunaway-Mariano, D., and Martin, B. M. (1995) *Biochemistry* **34,** 2181–2187
8. Carroll, L. J., Mehl, A. F., and Dunaway-Mariano, D. (1989) *J. Am. Chem. Soc.* **111,** 5965–5967
9. Pocalyko, D. J., Carroll, L. J., Martin, B. M., Babbitt, P. C., and Dunaway-Mariano, D. (1990) *Biochemistry* **29,** 10757–10765
10. Cleland, W. W. (1979) *Methods Enzymol.* **63,** 500–513
11. Howard, A. J., Gilliland, G. L., Finzel, B. C., Poulos, T. L., Ohlendorf, D. H., and Salemme, F. R. (1987) *J. Appl. Crystallogr.* **20,** 383–387
12. Brunger, A. T. (1992) *A System for X-ray Crystallography and NMR,* X-PLOR Version 3.1, Yale University, New Haven, CT
13. Roussel, A., and Cambillu, C. (1989) *Silicon Graphics Geometry Partner Directory*, TURBO_FRODO, Silicon Graphics, Mountain View, CA
14. Tronrud, D. E. (1992) *Acta Crystallogr. Sect. A* **48,** 912–916
15. Murzin, A. G. (1996) *Curr. Opin. Struct. Biol.* **6,** 386–394
16. Michaels, G., Milner, Y., Moskovitz, B. R., and Wood, H. G. (1978) *J. Biol. Chem.* **253,** 7656–7661
17. Mehl, A., Xu, Y., and Dunaway-Mariano, D. (1994) *Biochemistry* **33,** 1093–1102
18. Fan, C., Moews, P. C., Shi, Y., Walsh, C. T., and Knox, J. R. (1995) *Proc. Natl. Acad. Sci. U. S. A.* **92,** 1172–1176
19. Hara, T., Kato, H., Katsube, Y., and Oda, J. I. (1996) *Biochemistry* **35,** 11967–11974
20. Thoden, J. B., Wesenberg, G., Raushel, F. M., and Holden, H. M. (1999) *Biochemistry* **38,** 2347–2357
21. Joyce, M. A., Fraser, M. E., James, M. N. G., Bridger, W. A., and Wolodko, W. T. (2000) *Biochemistry* **39,** 17–25
22. Esser, L., Wang, C. R., Hosaka, M., Smagula, C. S., Sudhof, T. C., and Deisenhofer, J. (1998) *EMBO J.* **17,** 977–984
23. Wang, W. R., Kappock, T. J., Stubbe, J., and Ealick, S. E. (1998) *Biochemistry* **37,** 15647–15662
24. Thoden, J. B., Firestine, S., Nixon, A., Benkovic, S. J., and Holden, H. M. (2000) *Biochemistry* **39,** 8791–8802
25. Waldrop, G. L., Rayment, I., and Holden, H. M. (1994) *Biochemistry* **33,** 10249–10256
26. McGuire, M., Carroll, L. J., Yankie, L., Thrall, S. H., Dunaway-Mariano, D., Herzberg, O. Jayaram, B., and Haley, B. H. (1996) *Biochemistry* **35,** 8544–8552
27. Yankie, L., Xu, Y., and Dunaway-Mariano, D. (1995) *Biochemistry* **34,** 2188–2194
28. Fan, C., Park, I. S., Walsh, C. T., and Knox, J. R. (1997) *Biochemistry* **36,** 2531–2538
29. Thoden, J. B., Blanchard, C. Z., Holden, H. M., and Waldrop, G. L. (2000) *J. Biol. Chem.* **275,** 16183–16190

[7] By using the methods and reaction conditions described previously (6), we tested R92A, K22A, D321N, and E323D for their ability to catalyze single turnover reactions of [^{14}C]ATP in the presence and absence of P_i. The levels of [^{14}C]AMP detected in these reactions were too low be considered significant. Thus, it was concluded that these mutants are not effective at catalyzing the reaction ATP/P_i partial reactions. The relative contributions of reduced substrate/cofactor binding and altered internal equilibria to decreased product formation, however, are not known at this time.